Journal of
Materials Chemistry C

Accepted Manuscript

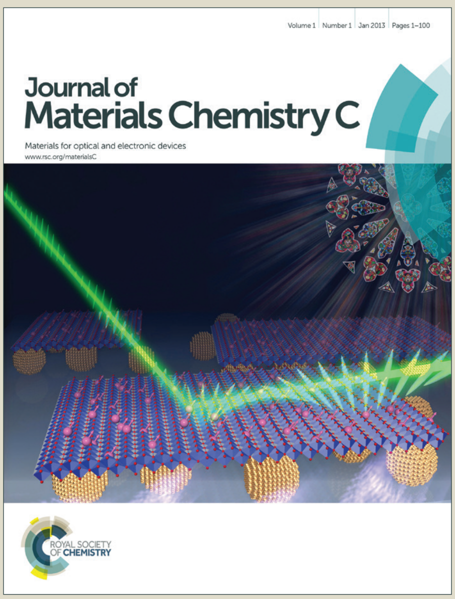

Cite this: DOI: 10.1039/c0xx00000x
www.rsc.org/xxxxxx
ARTICLE TYPE

Photoluminescence properties of Pr^{3+}, Sm^{3+} and Tb^{3+} doped $SrAlSi_4N_7$ and energy level locations of rare-earth ions in $SrAlSi_4N_7$

Zhi-Jun Zhang, [ab] **Otmar M. ten Kate,** [bc] **Anneke Delsing,**[b] **Pieter Dorenbos,** *[c] **Jing-Tai Zhao,** *[a] **and Hubertus T. Hintzen**[bc]

DOI: 10.1039/b000000x

ABSTRACT

RE^{3+} (RE = Pr, Sm, Tb) - doped $SrAlSi_4N_7$ samples were synthesized by a solid-state reaction method at high temperature, and their photoluminescence properties were investigated. It is noticeable that the 5*d* bands of Pr^{3+} and Tb^{3+} are at rather low energy in $SrAlSi_4N_7$ compared to oxides. Typical $4f^2 \rightarrow 4f^2$ emission lines (480 - 800 nm) of Pr^{3+} under $4f^2 \rightarrow 4f^1 5d^1$ excitation were observed in Pr^{3+}-doped $SrAlSi_4N_7$. Sm^{3+}-doped $SrAlSi_4N_7$ shows red emission originating from $^4G_{5/2} \rightarrow {}^6H_J$ (J = 5/2, 7/2 and 9/2) transitions, and the charge transfer band of Sm^{3+} was observed at an unusually low energy of 3.98 eV. Tb^{3+}-doped sample exhibits $^5D_3 \rightarrow {}^7F_J$ (J = 6, 5, 4, 3, 2, 1) (blue) and $^5D_4 \rightarrow {}^7F_J$ (J = 6, 5, 4, 3) (green) line emissions in the wavelength range of 375 - 650 nm under the direct Tb^{3+} $4f^8 \rightarrow 4f^7 5d^1$ excitation. The bands at about 256 nm in the excitation spectra are attributed to the host lattice absorption. In addition, there is energy transfer from the host lattice to the luminescent activators (Pr^{3+}, Sm^{3+}, Tb^{3+}). Energy level diagram containing the position of the 4*f* and 5*d* levels of all divalent and trivalent lanthanide ions relative to the valence and conduction band of $SrAlSi_4N_7$ has been constructed and discussed.

KEY WORDS: photoluminescence, $SrAlSi_4N_7$, rare earth, energy level

Introduction

Nitridosilicates, nitridoaluminosilicates and oxynitridosilicates have been widely utilized in structural ceramics and advanced optical materials due to their outstanding physical and chemical stabilities[1]. In the recent decades, silicon - nitride and -oxynitride based materials have been extensively investigated as host lattices for phosphors when activated by rare-earth ions, such as $SrAlSi_4N_7$: Eu^{2+} [2, 3], $SrAlSi_4N_7$: Ce^{3+}, Yb^{2+} [4, 5], $M_2Si_5N_8$: Eu^{2+}, Ce^{3+} (M = Ca, Sr, Ba) [6, 7], $MAlSiN_3$: Eu^{2+}, Ce^{3+} (M = Ca, Sr) [8, 9], $MSiN_2$: Eu^{2+}, Ce^{3+} (M = Ca, Sr, Ba) [10], α-SiAlON : RE (RE = Eu^{2+}, Ce^{3+}) [11, 12], $MSi_2O_{2-\delta}N_{2+2/3\delta}$: Eu^{2+}, Ce^{3+} (M = Ca, Sr, Ba) [13, 14], β-SiAlON : Eu^{2+} [15], $MSi_xAl_{2-x}O_{4-x}N_x$: Eu^{2+} (M = Ca, Sr, Ba) [16, 17]. These rare-earth doped silicon -nitrides and -oxynitrides have many advantages including strong absorption from UV to blue, high quantum efficiency, high chemical stability as well as excellent thermal quenching characteristics compared to oxide, sulfide and halide-based phosphors, allowing them to be widely used as efficient conversion phosphors for white-LEDs.

Recently, a new quaternary nitride system, $SrAlSi_4N_7$ has drawn much attention for its potential applications in the white-LEDs. When doped with Eu^{2+}, it exhibits bright orange-red emission under blue irradiation [2, 3]. $SrAlSi_4N_7$ shows no structural resemblance to $MLnSi_4N_7$ (M = Sr, Ba, Ln = Y, Yb), but crystallizes in the $Pna2_1$ space group [2]. According to the research work reported by Hetch *et al* [2], the crystal structure of $SrAlSi_4N_7$ is comprised of both corner-sharing SiN_4 and AlN_4 tetrahedra and edge-sharing AlN_4 tetrahedra. More intriguingly, infinite chains running along [001] are built of edge-sharing AlN_4 tetrahedra, and the chains are connected with corner-sharing SiN_4 tetrahedra. Two different Sr^{2+} atoms coordinated by six or eight N atoms are hosted in the channels. At the smaller Sr site (Sr1), the shortest Sr-N distance is 2.499 Å and the average distance to the nearest six nitrogen anions is 2.701 Å. At the larger Sr site (Sr2), the shortest Sr-N distance is 2.642 Å and the average distance to the eight nearest nitrogen anions is 2.865 Å. When $SrAlSi_4N_7$ is doped with Ce^{3+} or Yb^{2+}, it exhibits bright yellow-red emission under blue light [4, 5]. Furthermore, a warm white-light LED can be generated by using single $SrAlSi_4N_7$: Ce^{3+}/Yb^{2+} as the wavelength conversion phosphor combined with a blue LED chip (InGaN) [5]. Herein, we focus on investigating the photoluminescence properties of rare-earth ions (RE = Pr, Sm, Tb) in $SrAlSi_4N_7$, and the luminescence mechanism of these rare-earth ions in $SrAlSi_4N_7$ will be studied.

Experimental details

Starting Materials

The binary nitride precursor SrN_x ($x \approx 0.6$ - 0.66) was pre-prepared by the reaction of the pure strontium metal (Aldrich, 99.9 %, pieces) under flowing dried nitrogen at 850 °C for 15 hours in horizontal tube furnaces. In addition, AlN (Tokuyama Chemical Co., Ltd., F-grade), α-Si_3N_4 (Permascand, P95H, α content, 93.2 wt%, oxygen content: ~ 1.5 wt%), Li_3N (Aldrich, purity 99 %), Pr, Sm and Tb metal powder (Alfa, > 99 %, lumps) are used as the as-received raw materials.

Synthesis of $Sr_{0.94}RE_{0.03}Li_{0.03}AlSi_4N_7$ (RE = Pr, Sm, Tb)

$Sr_{0.94}RE_{0.03}Li_{0.03}AlSi_4N_7$ (RE = Pr, Sm, Tb) powder samples were prepared by solid-state reaction at high temperature. Appropriate amounts of starting materials were weighed, thoroughly mixed and ground in an agate mortar. The powder mixtures were fired in

Cite this: DOI: 10.1039/c0xx00000x

www.rsc.org/xxxxxx

ARTICLE TYPE

molybdenum crucibles at 1600 °C for 16 h in a horizontal tube furnace under N_2 - H_2 (5 vol.%) atmosphere. After firing, the samples were gradually cooled down in the furnace. Subsequently, the resulting powder was reground and then fired at 1600 °C for 16 h in a molybdenum crucible under flowing N_2-H_2 (5 vol.%) atmosphere. After sintering, these samples were gradually cooled down to room temperature in the furnace. There was no apparent reaction of the prepared samples with the Mo crucibles. All processes were handled in a dry glovebox flushed with dry nitrogen because of air and water sensitivity of some starting materials.

X-ray diffraction data collection and analysis

All measurements were performed on finely ground samples, which were analyzed by X-ray powder diffraction (Bruker, D4 Endeavor X-ray Diffractometer) using CuK_{α} radiation at 40 kV and 40 mA with a graphite monochromator. The 2θ ranges of all the data sets are from 10 to 80° using step scan with a step size of 0.02 ° in 2θ and a count time of 1 second per step. The XRD measurements were performed at room temperature in air.

Optical measurements

The diffuse reflectance spectra in the UV and visible range of Pr^{3+}, Sm^{3+} and Tb^{3+}-doped $SrAlSi_4N_7$ were measured at room temperature by a Perkin Elmer LS 50B spectrophotometer equipped with a Xe flash lamp and an R952 photomultiplier. The reflection spectra were calibrated with the reflection of black felt (reflection 3 %) and white barium sulfate ($BaSO_4$, reflection ~ 100 %) in the wavelength region of 230 - 700 nm. The diffuse reflectance spectra in the infrared range were recorded with a Bruker Vertex 80v FT interferometer using tungsten as a light source and a cooled InGaAs and Si detector. Excitation and emission spectra were recorded with a xenon light source with a double gating monochromator and a Hamamatsu EM CCD camera C9100-13. The excitation spectra were corrected for the lamp intensity, and the emission spectra were corrected for detector sensitivity and transmission of emission monochromator. All luminescence spectra were measured with a scan speed of 400 nm/min at room temperature in air.

Results and discussion

Phase formation of $Sr_{0.94}RE_{0.03}Li_{0.03}AlSi_4N_7$ (RE = Pr, Sm, Tb)

Fig. 1 shows the powder XRD patterns of RE (RE = Pr, Sm, Tb) doped $SrAlSi_4N_7$ samples. The XRD patterns are in good agreement with standard $SrAlSi_4N_7$ (ICSD no. 163667). The ionic radii of Pr^{3+} (r = 0.99 Å, CN = 6; r = 1.126 Å, CN = 8), Sm^{3+} (r = 0.958 Å, CN = 6; r = 1.079 Å, CN = 8) and Tb^{3+} (r = 0.923 Å, CN = 6; r = 1.04 Å, CN = 8) are smaller than that of Sr^{2+} (r = 1.18 Å, CN = 6; r = 1.26 Å, CN = 8), but much larger than Al^{3+} (r = 0.39 Å, CN = 4) [18]. As a consequence, the Sr^{2+} sites (Sr1 and/or Sr2) could be substituted by RE^{3+}, as will be further discussed.

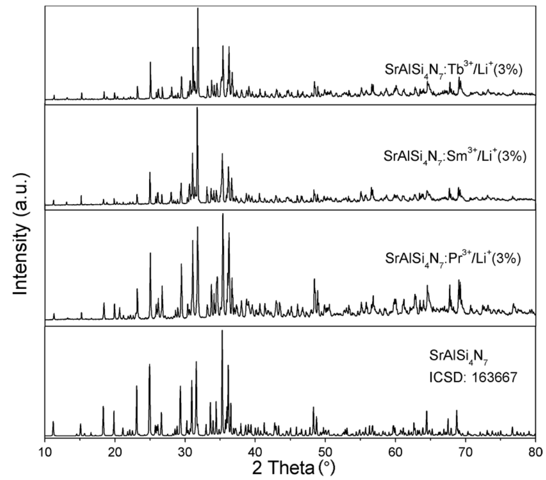

Fig. 1 X-ray powder diffraction patterns of $SrAlSi_4N_7$, $Sr_{0.94}Pr_{0.03}Li_{0.03}AlSi_4N_7$, $Sr_{0.94}Sm_{0.03}Li_{0.03}AlSi_4N_7$, and $Sr_{0.94}Tb_{0.03}Li_{0.03}AlSi_4N_7$.

Diffuse reflection spectra of $Sr_{0.94}RE_{0.03}Li_{0.03}AlSi_4N_7$ (RE = Pr, Sm, Tb)

The diffuse reflection spectrum of $Sr_{0.94}Pr_{0.03}Li_{0.03}AlSi_4N_7$ is shown in Fig. 2 (solid line). There is a broad intense absorption band at about 300 nm originating from Pr^{3+} ions ($4f^2 \rightarrow 4f^1 5d^1$ transition). The optical absorption edge at the short-wavelength (i.e. higher energy) in the wavelength range 250 - 290 nm in the reflection spectrum can be attributed to the valence-to-conduction band transitions of the $SrAlSi_4N_7$ host lattice. Several weak absorption lines at longer-wavelength (i.e. lower energy) can be seen in the range of 438 - 525 nm as well as 582 - 620 nm (Fig. 2), which are attributed to the $^3H_4 \rightarrow {}^3P_2$ (~ 458 nm), $^3H_4 \rightarrow {}^3P_1$ (~ 485 nm) and $^3H_4 \rightarrow {}^3P_0$ (~ 500 - 512 nm) transitions of Pr^{3+} ions, respectively.
The absorption spectrum of $SrAlSi_4N_7$ was obtained from the reflection spectrum by using the Kubelka - Munk function [19]:

$$F(R) = (1-R)^2/2R = K/S \qquad (1)$$

R, K, and S are the reflection, the absorption coefficient, and the scattering coefficient, respectively. The absorption (K/S) spectrum of $SrAlSi_4N_7$ derived with the Kubelka - Munk function, as shown in the inset in Fig. 2, is used to determine the thresholds for host lattice absorption. The value of the optical absorption edge of $SrAlSi_4N_7$ is calculated to be about 4.8 eV (i.e. 260 nm) by extrapolating the Kubelka - Munk function to K/S = 0. Moreover, another broad absorption band in the wavelength range of 290 - 350 nm is observed.

Cite this: DOI: 10.1039/c0xx00000x

www.rsc.org/xxxxxx

ARTICLE TYPE

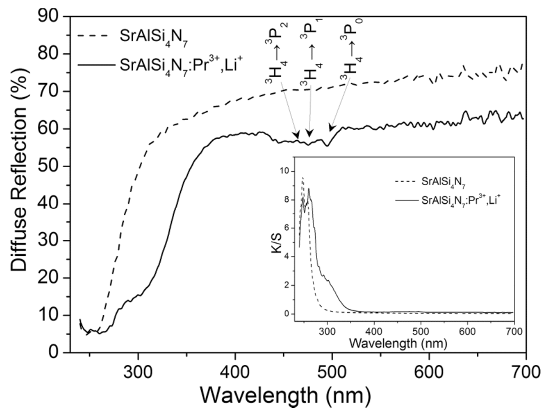

Fig. 2. The diffuse reflection spectra of $SrAlSi_4N_7$ (dash line) and $Sr_{0.94}Pr_{0.03}Li_{0.03}AlSi_4N_7$ (solid line) (The inset shows the absorption spectra as calculated by the Kubelka - Munk formula).

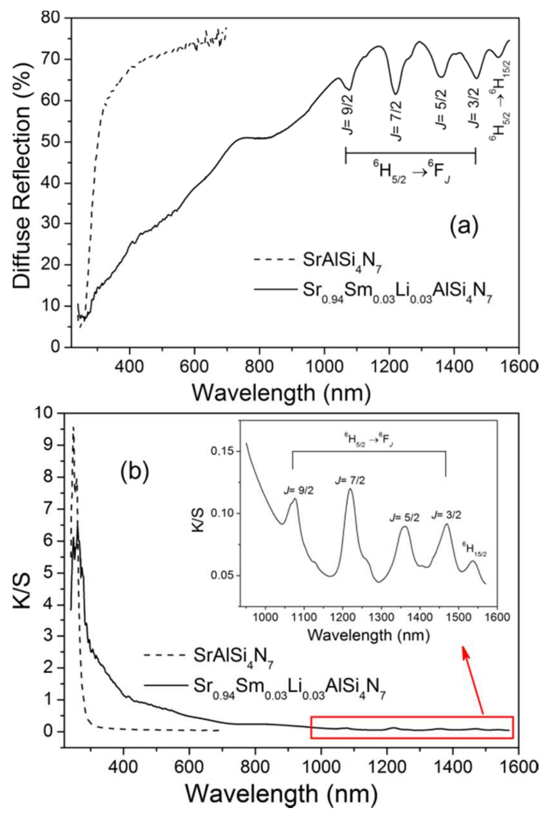

Fig. 3. The diffuse reflection spectra of $SrAlSi_4N_7$ (dash line) and $Sr_{0.94}Sm_{0.03}Li_{0.03}AlSi_4N_7$ (solid line) (a), the absorption spectra as calculated by the Kubelka - Munk formula (b) (the inset shows enlarged absorption peaks of Sm^{3+}).

The diffuse reflection spectrum of $Sr_{0.94}Sm_{0.03}Li_{0.03}AlSi_4N_7$ is shown in Fig. 3(a). In the infrared region, *f* - *f* line absorption of Sm^{3+} can be observed from the $^6H_{5/2}$ ground state to the $^6H_{15/2}$ (1538 nm), $^6F_{3/2}$ (1468 nm), $^6F_{5/2}$ (1362 nm), $^6F_{7/2}$ (1220 nm, 1260 nm) and $^6F_{9/2}$ (1075 nm) states. In the UV and visible range, a broad absorption band is observed in the range from 230 nm to 400 nm, which can ascribed to the charge transfer band (CTB) of Sm^{3+} ions. This observation will be confirmed by the excitation spectra discussed below. There is no sign for the existence of Sm^{2+}, due to the absence of Sm^{2+} *f* - *f* absorption lines in the diffuse reflection spectrum. The absorption (*K*/*S*) spectrum of $Sr_{0.94}Sm_{0.03}Li_{0.03}AlSi_4N_7$ derived with the Kubelka - Munk function is shown in Fig. 3(b).

For Tb^{3+} - doped $SrAlSi_4N_7$, there is a weak absorption band in the wavelength range of 270 - 310 nm, which can be attributed to the transitions from the $4f^8$ ground state of Tb^{3+} to its $4f^75d^1$ excited states (Fig. 4). A short wavelength (i.e. higher energy) absorption around 225 - 275 nm in the diffuse reflection spectrum can be ascribed to the absorption of the host lattice (as discussed in $Sr_{0.94}Pr_{0.03}Li_{0.03}AlSi_4N_7$ and $Sr_{0.94}Sm_{0.03}Li_{0.03}AlSi_4N_7$). The absorption (*K*/*S*) spectrum of $Sr_{0.94}Tb_{0.03}Li_{0.03}AlSi_4N_7$ derived with the Kubelka - Munk function is shown in the inset in Fig. 4.

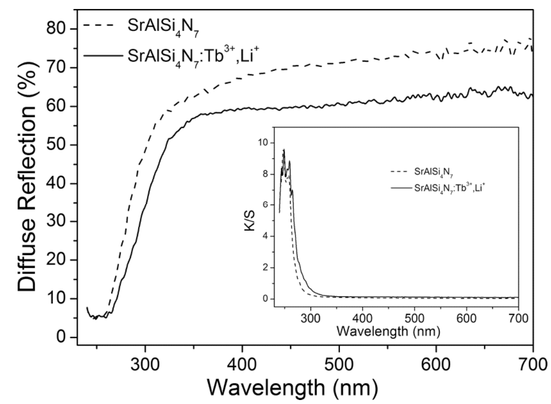

Fig. 4. The diffuse reflection spectra of $SrAlSi_4N_7$ (dash line) and $Sr_{0.94}Tb_{0.03}Li_{0.03}AlSi_4N_7$ (solid line) (The inset shows the absorption spectra as calculated by the Kubelka - Munk formula).

Photoluminescence of $Sr_{0.94}Pr_{0.03}Li_{0.03}AlSi_4N_7$

The energy level structure of the Pr^{3+} ion with two 4*f* electrons ($4f^2$) introduces several 4*f* - 4*f* transitions [20]. Fig. 5 shows the typical excitation and emission spectra of $SrAlSi_4N_7$: Pr^{3+}/Li^+ (3 %). There are three possible 4*f* emitting states for the Pr^{3+} ion, i.e. $^3P_0$, $^1D_2$ and $^1G_4$ levels, and the emission color of Pr^{3+} depends on the intensity ratio of $4f^2 \rightarrow 4f^2$ transitions at a fixed energy, which is strongly affected by the host lattice. Under direct $4f^2 \rightarrow 4f^15d^1$ excitation of Pr^{3+} around 320 nm, typical $4f^2 \rightarrow 4f^2$ emission lines of Pr^{3+} in the wavelength range of 400 - 1050 nm are observed in the emission spectra (Fig. 5(b)), which can be assigned to $^3P_0 \rightarrow {}^3H_4$ (~ 500, 512 nm), $^3P_0 \rightarrow {}^3H_5$ (~ 550 nm), $^1D_2 \rightarrow {}^3H_4$ (~ 612 nm), $^3P_0 \rightarrow {}^3H_6$ (~ 629 nm), $^3P_0 \rightarrow {}^3F_2$ (~ 667 nm), $^3P_0 \rightarrow {}^3F_3$ (~ 705 nm) and $^3P_0 \rightarrow {}^3F_4$ (~ 745 nm) transitions, respectively. The predominant emission is the $^1D_2 \rightarrow {}^3H_4$ transition at about 612 nm. However, the $4f^15d^1 \rightarrow 4f^2$ emission of Pr^{3+} has not been observed in the emission spectra, even though the lowest $4f^15d^1$ state (~33,780 cm^{-1}, which will be discussed below) of Pr^{3+} in $SrAlSi_4N_7$ is lower than the $4f^2$ excited [$^1S_0$] level (at ~ 46,800 cm^{-1}). It is probably due to the very large redshift, and the emission is quenched by relaxation to the ^3P levels. On the other hand, as shown in Fig. 5 (b), typical $4f^2 \rightarrow 4f^2$ emissions of Pr^{3+} are also observed under 255 nm excitation, which means that the energy transfer from the host lattice to Pr^{3+} ions does exist.

Cite this: DOI: 10.1039/c0xx00000x

www.rsc.org/xxxxxx

ARTICLE TYPE

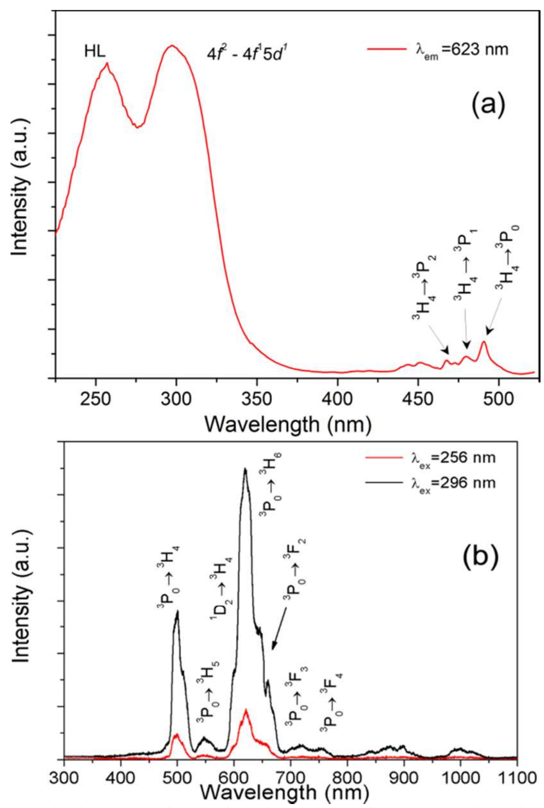

Fig. 5. Excitation (a) and emission (b) spectra of $Sr_{0.94}Pr_{0.03}Li_{0.03}AlSi_4N_7$.

Excitation spectra monitoring the $4f^2 \rightarrow 4f^2$ emissions are also shown in Fig. 5 (a). There are two principle strong excitation bands. One is the excitation band below 280 nm with the peak at 258 nm originating from host lattice excitation, which can be ascribed to the host lattice excitation caused by charge transfer within the Si/Al - N network, in agreement with the observation in the diffuse reflection spectra. The second broad excitation band is in the range from 280 - 375 nm with a maximum at about 296 nm which is related to the strong $4f^2 \rightarrow 4f^15d^1$ transition of Pr^{3+} ions in the host lattice. In addition, a group of weak $4f^2 \rightarrow 4f^2$ transitions ($^3H_4 \rightarrow {}^3P_0$, $^3H_4 \rightarrow {}^3P_1$ and $^3H_4 \rightarrow {}^3P_2$) of Pr^{3+} can be observed in the range of 438 - 525 nm in the excitation spectra, which is consistent with the diffuse reflectance spectra.

It is well known that the $5d$ levels of RE^{3+} ions in a specific host lattice are at lower energy compared to the $5d$ orbital energy of the free RE^{3+} ions due to nephelauxetic and crystal field splitting effects [21-23]. Dorenbos provided the $4f$ - $5d$ transition energies of triply ionized lanthanides in various compounds and proposed that the crystal field and covalency decrease D(Ln, *A*) for the energy of the $4f^{n-1}5d$ levels of a lanthanide ion in compound *A* relative to the energies in the free ion, i.e.

$$D(Ln, A) = E(Ln, free) - E(Ln, A) \qquad (2)$$

is almost independent of the nature of the lanthanide ion doped.

Here, E(Ln, free) is the energy of the first f - d transition of Ln^{3+} as free (gaseous) ion. E(Ln, *A*) is the energy of the first f - d transition of the lanthanide ion Ln^{3+} doped in compound *A*. The lowest $4f$ - $5d$ excitation transition of Ce^{3+}, E(Ce^{3+}, $SrAlSi_4N_7$) was found to be 434 nm (i.e. 23,040 cm^{-1}) [5]. The $5d$ level of the free Ce^{3+} ion is 49,340 cm^{-1} [21]. So, the f - d transition energy of Ce^{3+} in $SrAlSi_4N_7$ is decreased by 26,300 cm^{-1}, compared to that of the free Ce^{3+} ion, implying that D(Ce^{3+}, $SrAlSi_4N_7$) is about 26,300 cm^{-1}.

Because the influence of the crystal field and covalency of the host lattice on the red shift of the $5d$ levels is approximately equal for all RE ions [21], the crystal field and covalency decrease D(Ce^{3+}, $SrAlSi_4N_7$) for the energy of the $4f^{n-1}5d$ levels of Ce^{3+} in $SrAlSi_4N_7$ can be used to predict the $5d$ energies of other lanthanides. The $4f$ - $5d$ transition for the free Pr^{3+} ion is 61,580 cm^{-1} [21]. Therefore, the lowest f - d transition energy E(Pr^{3+}, $SrAlSi_4N_7$) of Pr^{3+} in $SrAlSi_4N_7$ is estimated at 35,280 cm^{-1} (284 nm) according to Eq. (2), in agreement with the experimental results (296 nm, or 33,780 cm^{-1}).

Photoluminescence of $Sr_{0.94}Sm_{0.03}Li_{0.03}AlSi_4N_7$

Trivalent Sm^{3+} with $4f^5$ configuration exhibits a more complicated energy level structure and various possible transitions between f levels [24, 25]. As a consequence, the $4f$ - $4f$ transitions give rise to sharp line emissions. Divalent Sm^{2+} has the $4f^6$ electron configuration, which under irradiation with UV and visible light can be excited into the $4f^55d^1$ levels.

The excitation and emission spectra of $Sr_{1-2x}Sm_xLi_xAlSi_4N_7$ (x = 0.03) are shown in Fig. 6. The excitation spectrum of $Sr_{0.94}Sm_{0.03}Li_{0.03}AlSi_4N_7$ was recorded by monitoring the line emission of $^4G_{5/2} \rightarrow {}^6H_{9/2}$ (650 nm) of Sm^{3+}. The excitation spectrum consists of one broad excitation band corresponding to the absorption bands observed in the diffuse reflection spectrum. This broad band at 312 nm (FWHM ~ 1 eV) cannot be due to the $4f \rightarrow 5d$ transition for Sm^{3+}, because its energy can be calculated by Eq. (2) to be about 49,540 cm^{-1} (202 nm) using a D($SrAlSi_4N_7$) value of 26,300 cm^{-1} and the free Sm^{3+} ion $4f \rightarrow 5d$ energy of 75,840 cm^{-1} [22]. Therefore, the broad excitation band at about 312 nm (~ 3.98 eV) is attributed to the charge transfer band (CTB) of Sm^{3+} ions in $SrAlSi_4N_7$, which is similar to the result of $N^{3-} \rightarrow Sm^{3+}$ charge transfer transition in $CaAlSiN_3$ (318 nm / 3.91 eV) [26] and Ca-α-Sialon (308 nm / 4.03 eV) [27]. The energy of the $N^{3-} \rightarrow Sm^{3+}$ charge transfer band (~ 4 eV) is lower than that of the $O^{2-} \rightarrow Sm^{3+}$ charge transfer band (> 5 eV) [28], which is attributed to the lower electronegativity of N versus O. In addition, the peaks observed in the excitation spectrum in the region of 300 - 500 nm are due to the excitation from the ground-level $^6H_{5/2}$ to higher energy levels ($^4F_{9/2}$, $^4K_{13/2}$, $^4L_{17/2}$, $^6P_{7/2}$, $^4D_{1/2}$, $^4K_{11/2}$, $^6P_{3/2}$, $^4M_{21/2}$, $^4F_{7/2}$, $^4M_{19/2}$, $^4I_{15/2}$, $^4G_{9/2}$) characteristic for Sm^{3+}.

Cite this: DOI: 10.1039/c0xx00000x

www.rsc.org/xxxxxx

ARTICLE TYPE

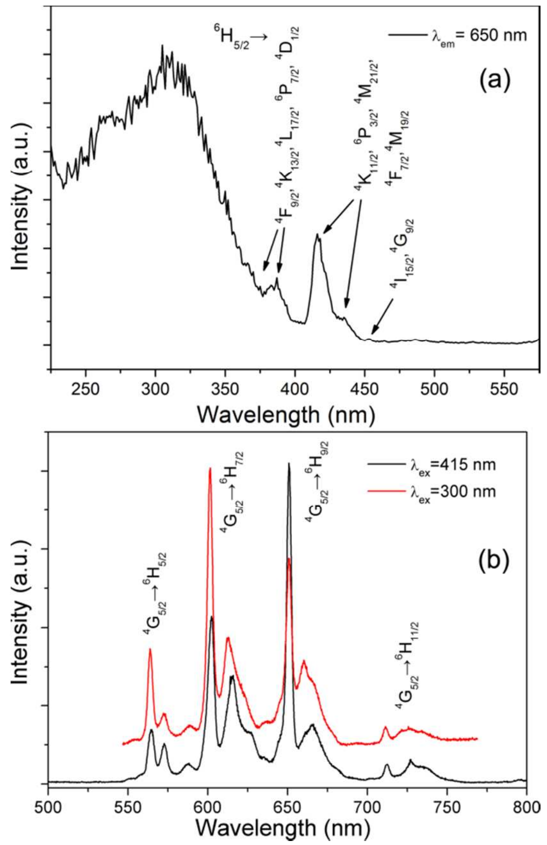

Fig. 6. The excitation (a) and emission (b) spectra of $Sr_{0.94}Sm_{0.03}Li_{0.03}AlSi_4N_7$.

As illustrated in Fig. 6 (b), $Sr_{0.94}Sm_{0.03}Li_{0.03}AlSi_4N_7$ exhibits bright red emission under 300 and 415 nm excitation. The emission spectra are composed of peaks at about 570, 610, 650 and 710 nm, corresponding to the $^4G_{5/2} \rightarrow {}^6H_J$ (J = 5/2, 7/2, 9/2 and 11/2) transitions of Sm^{3+}. Among them, the red emission $^4G_{5/2} \rightarrow {}^6H_{7/2}$ and $^4G_{5/2} \rightarrow {}^6H_{9/2}$ exhibits the strongest intensity under 300 and 415 nm excitation. There is no clear-cut evidence for the presence of Sm^{2+}, since no transitions of Sm^{2+} could be identified.

Photoluminescence of $Sr_{0.94}Tb_{0.03}Li_{0.03}AlSi_4N_7$

$Sr_{0.94}Tb_{0.03}Li_{0.03}AlSi_4N_7$ emits bright blue-green light under 255, 278 and 324 nm excitation (Fig. 7 (b)). The emission spectrum of Tb^{3+} in $SrAlSi_4N_7$ is composed of two groups of lines in the wavelength range of 350 - 700 nm: one group in the wavelength range 490 - 700 nm corresponding to the $^5D_4 \rightarrow {}^7F_J$ (J = 6, 5, 4, 3) transitions of Tb^{3+}, and the other group of relatively weak peaks in the wavelength range 350 - 490 nm originating from the $^5D_3 \rightarrow {}^7F_J$ (J = 6, 5, 4, 3, 2, 1, 0) transitions of Tb^{3+}. The predominant emission is the $^5D_4 \rightarrow {}^7F_5$ transition at about 545 nm. The relative intensities of the $^5D_4$ and $^5D_3$ emissions for Tb^{3+} - activated samples strongly depend on the Tb^{3+} concentration. Normally, a blue emission originating from the $^5D_3$ level is observed at low Tb^{3+} concentration. If other Tb^{3+} ions are present at short distances (high Tb^{3+} concentration), non-radiative decay from the $^5D_3$ state to $^5D_4$ state via cross relaxation ($^5D_3 \rightarrow {}^5D_4 \Rightarrow {}^7F_6 \rightarrow {}^7F_0$ and/or $^5D_3 \rightarrow {}^7F_0 \Rightarrow {}^7F_6 \rightarrow {}^5D_4$) is possible, resulting in a change from blue to green emission [29]. This change is observed if, for a system of homogeneously distributed Tb^{3+} ions, the Tb^{3+} concentration is increased above the critical Tb^{3+} concentration for cross-relaxation [30]. For $Sr_{0.94}Tb_{0.03}Li_{0.03}AlSi_4N_7$, the emission is dominantly green which suggests that clustering or pair formation of Tb^{3+} ions does not occur. The excitation of 324 nm introduces the same position of emission peaks compared to 278 nm excitation, but quite different relative luminescence intensities. The emissions from the $^5D_4$ state are relatively strong compared to that of the $^5D_3$ state after excitation at high energy (278 nm), however, after excitation at low energy (324 nm) the blue emissions from the $^5D_3$ state almost disappear but the green emissions from the $^5D_4$ state are still strong.

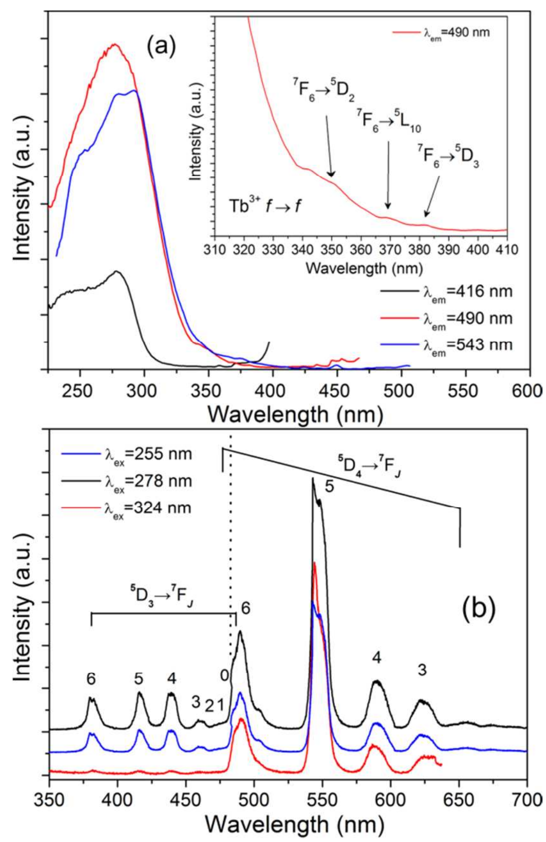

Fig. 7. The excitation (a) and emission (b) spectra of $Sr_{0.94}Tb_{0.03}Li_{0.03}AlSi_4N_7$.

The excitation spectra of $Sr_{0.94}Tb_{0.03}Li_{0.03}AlSi_4N_7$ consist of one broad band in the wavelength range of 225 - 350 nm (as shown in Fig. 7(a)). This UV excitation band is attributed to overlapping transitions from the valence to conduction bands of the host lattice of $SrAlSi_4N_7$ and from the $4f \rightarrow 5d$ transition of Tb^{3+}. The excitation band below 270 nm with the peak at 256 nm is not due to the absorption of Tb^{3+} since this peak at this wavelength can also be observed in RE (RE = Pr, Sm, Tb, Yb) -doped $SrAlSi_4N_7$. The broad band at 256 nm is assigned to the host lattice excitation corresponding to the absorption band observed in the diffuse reflection spectrum. In both excitation spectra a broad excitation band with the maximum at about 278 nm is observed, which is

Cite this: DOI: 10.1039/c0xx00000x

www.rsc.org/xxxxxx

ARTICLE TYPE

related to the $4f \rightarrow 5d$ ($4f^8 \rightarrow 4f^7 5d^1$) spin-allowed transition of Tb^{3+} in the host. The excitation spectrum of the $^5D_4 \rightarrow {}^7F_5$ emission exhibits the same peak position and shape with the excitation spectrum of the $^5D_3 \rightarrow {}^7F_5$ emission, indicating that one Tb^{3+} luminescent center is present in $SrAlSi_4N_7$. The spin-allowed $4f \rightarrow 5d$ transition for the free Tb^{3+} ion is reported to be 62,500 cm^{-1} [21]. Therefore, the spin-allowed $4f \rightarrow 5d$ transition energy E(Tb^{3+}, $SrAlSi_4N_7$) of the Tb^{3+} in $SrAlSi_4N_7$ can be calculated to be about 36,200 cm^{-1} (276 nm) according to Eq. (2), in excellent agreement with the experimental results (278 nm). In addition, some very weak sharp lines in the wavelength range of 335 - 475 nm are observed, which can be ascribed to the transitions between the energy levels within the $4f^8$ configuration, i.e. $^7F_6 \rightarrow {}^5D_3$ (~ 380 nm), $^7F_6 \rightarrow {}^5L_{10}$ (~ 368 nm) and $^7F_6 \rightarrow {}^5D_2$ (~ 354 nm), as shown in the inset of Fig. 7 (a).

Energy level diagram of lanthanides in $SrAlSi_4N_7$

The luminescence properties of all divalent and trivalent lanthanides in a specific host lattice can be related to each other according to the energy level diagram, which is originally developed by Dorenbos [21, 28, 31, 32]. However, it is necessary to clarify the site occupation of the lanthanide ions before the construction of the energy level diagram, since there are two different Sr^{2+} sites (Sr1, Sr2) in $SrAlSi_4N_7$. In our previous research work, the single type of Ce^{3+} center in $SrAlSi_4N_7$ was verified by the decomposition of emission spectra and the fluorescent life time of Ce^{3+} [5]. Moreover, as indicated above, only one Tb^{3+} luminescent center is present in $SrAlSi_4N_7$ according to the excitation spectra. Possible explanation is that the smaller Sr^{2+} site (Sr1) seems to be preferentially occupied by the trivalent lanthanide ions because the ionic sizes of the trivalent lanthanide ions (Ce^{3+}, Pr^{3+}, Sm^{3+}, Tb^{3+}) are smaller than that of Sr^{2+}. In addition, Li^+ was added with the trivalent lanthanide ion for charge compensation, introducing even smaller "average" Ln^{3+}/Li^+ radius as compared to the trivalent lanthanide ion itself. But the situation for the divalent lanthanide ions is completely different since no Li^+ is required for charge compensation and moreover the divalent lanthanide ions are significantly larger than the trivalent lanthanide ions. For example, the radius of Eu^{2+} is similar to that of Sr^{2+}, resulting most probably in 2 Sr^{2+} sites (Sr1, Sr2) occupation in $SrAlSi_4N_7$ because there is some evidence of a weak second site emission at shorter wavelength (higher energy) than the main site emission at longer wavelength (lower energy) [17]. While the ionic size of Yb^{2+} is still smaller than that of Sr^{2+}, making probable the preferential occupation of the smaller Sr^{2+} site (Sr1), as observed in our previous work [5]. Therefore, a detailed energy level scheme (Fig. 8) which shows the energy of the $4f$ and $5d$ states of all divalent and trivalent lanthanides relative to the valence and conduction band of $SrAlSi_4N_7$ can be constructed by virtue of the optical and luminescence spectroscopy data of Ln^{2+} and Ln^{3+} ions located on the smaller Sr^{2+} site (Sr1) in $SrAlSi_4N_7$.

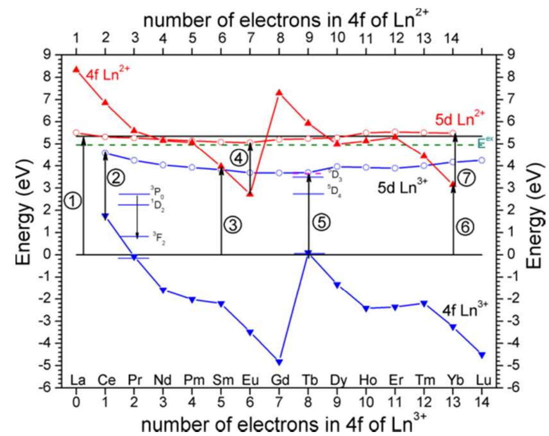

Fig. 8 Energy level scheme showing the $4f$ ground states of the trivalent (▼) and divalent ions (▲) and lowest energy $5d$ states of the trivalent (○) and divalent ions (○) relative to the valence and conduction band of $SrAlSi_4N_7$. The arrows (1-6) indicate the experimentally determined optical transition used to construct this scheme.

Accordingly, several different experimentally determined optical and luminescence spectroscopy data were chosen to construct the energy level diagram for $SrAlSi_4N_7$: (i) the band gap (5.35 eV) of $SrAlSi_4N_7$ (arrow 1) [5], (ii) the Ce^{3+} $4f$ - $5d$ absorption (arrow 2) [5], (iii) the charge transfer band of Sm^{3+} (arrow 3) (this work), (iv) the f - d absorption of Eu^{2+} (arrow 4) [2], (v) the lowest energy (i.e.spin-forbidden) $4f \rightarrow 5d$ transition of Tb^{3+} (arrow 5) (this work) and (vi) the charge transfer band of Yb^{3+} (arrow 6) [5]. The band gap is defined as the energy of charge transfer from the top of the valence band to the bottom of the conduction band. The value of band gap is the same as the energy of the host lattice excitation band at 4.96 eV plus an estimated 0.39 eV for the exciton binding energy. The energy difference between the lowest $4f$ and lowest $5d$ states of the trivalent lanthanide ions can be derived from both the excitation spectrum of the Ce^{3+} d - f emission band, as well as the excitation spectrum of the Tb^{3+} f - f emission lines, since in both excitation spectra an f - d transition band is observed. It is known that the spin-forbidden $4f \rightarrow 5d$ transition is at about 0.8 eV lower energy than the spin-allowed transition [32]. In Tb^{3+}-doped $SrAlSi_4N_7$, the Tb^{3+} spin-allowed $4f \rightarrow 5d$ transition is located at about 278 nm (i.e. 4.47 eV), thus the spin-forbidden $4f \rightarrow 5d$ transition of Tb^{3+} is expected to be at 3.67 eV, as illustrated (arrow 5) in Fig. 8. The data on the charge transfer band of any tetravalent lanthanide ion which relates the lowest $4f$ of the trivalent ion level to the top of the valence band, or the thermal quenching data on the d - f emission of the trivalent lanthanide ion which relate the $5d$ levels to the bottom of the conduction band, is needed to position the energy levels of the trivalent ions with respect to the valence and conduction band. Because there is no information about the CT energy of any tetravalent lanthanide ion, an indication on the energy difference between the $4f$ ground state of Ln^{3+} and the top of the valence band can be obtained from luminescence temperature quenching data of the Ce^{3+} d - f emission in $SrAlSi_4N_7$. The position of the lowest Ce^{3+} $5d$ level is roughly estimated to be at least about 0.52 eV below the bottom of the conduction band, deducing from the thermal quenching data of Ce^{3+} [5]. The energy of the Yb^{3+} CT band

Cite this: DOI: 10.1039/c0xx00000x

www.rsc.org/xxxxxx

ARTICLE TYPE

(3.15 eV) equals the energy difference between the 4*f* ground state of Yb^{2+} and the top of the valence band (arrow 6). The wavelength of the first $4f^7$ - $4f^6 5d$ transition in Eu^{2+}, is estimated near 550 nm from the Eu^{2+} excitation spectra from Hecht *et al* [2]. The corresponding energy of 2.34 eV (arrow 4) then provides the energy difference between the lowest 4*f* and lowest 5*d* states of all other divalent ions. So, the *f* - *d* transition of Yb^{2+} can be predicted to be 2.35 eV (arrow 7), which is in good agreement with the value (2.36 eV) observed in our previous work [5].
Furthermore, the energy scheme is also a powerful tool to interpret the preferred divalent and trivalent states of lanthanide ions in $SrAlSi_4N_7$. When the energy difference between the ground state of the divalent ion and the bottom of the conduction band is large, the divalent ion will be more stable and it will be more likely that the divalent ion is formed during synthesis [33]. So, as shown in Fig. 8, the 4*f* ground state of Eu^{2+} is slightly closer to the valence band than to the conduction band, and all europium is found in the divalent state (Eu^{2+}) rather than trivalent state (Eu^{3+}). However, the 4*f* ground state of Sm^{2+} is 1.25 eV higher in energy than that of Eu^{2+} and therefore closer to the conduction band than to the valence band. Sm is expected to be stable in the trivalent state in $SrAlSi_4N_7$, which has been verified by our research aforementioned. Despite using a reducing atmosphere N_2 - H_2 (5 vol.%), Sm^{3+} was not converted into Sm^{2+}. Apparently, Tm should exists in the trivalent state in $SrAlSi_4N_7$ because the 4*f* state of Tm^{2+} is 1.72 eV higher in energy than that of Eu^{2+}. The 4*f* ground state of Yb^{2+} is slightly closer to the conduction band than the distance to the top of valence band, therefore, Yb is expected to be also stable in the trivalent state besides the divalent state as indeed observed [5]. What's more, Yb^{2+} ions do not require charge compensation, and they show similar ionic size to that of Sr^{2+}, while Yb^{3+} is much smaller.

Conclusions

In summary, $Sr_{.94}RE_{0.03}Li_{0.03}AlSi_4N_7$ (RE = Pr, Sm and Tb) samples were prepared by a solid-state reaction at high temperature, and their photoluminescence properties were studied. The host absorption band is located at about 258 nm. 5*d* bands of Pr^{3+} and Tb^{3+} are at rather low energy in $SrAlSi_4N_7$ due to strong nephelauxetic effect and crystal field splitting originating from coordination with N^{3-} ions. Strong typical $4f^2 \rightarrow 4f^2$ emission lines (450 - 800 nm) of Pr^{3+} are observed under the direct $4f^2 \rightarrow 4f^1 5d^1$ excitation at 296 nm. The charge transfer band of Sm^{3+} located at about 315 nm is rather low because of a lower electronegativity of N compared with O. The spin-allowed $f \rightarrow d$ transition of Tb^{3+} in $SrAlSi_4N_7$ is observed at 278 nm, and the characteristic Tb^{3+} emission lines from $^5D_3$ or $^5D_4$ to ^7F_J levels were observed. An energy level scheme showing the positions of the 4*f* and 5*d* energy levels of all divalent and trivalent lanthanide ions relative to the valence and conduction band of the $SrAlSi_4N_7$ phosphors has been constructed and explained.

Acknowledgements

The authors gratefully acknowledge financial support from the European Union, the Freistaat Thüringen and the Leuchtstoffwerk Breitungen GmbH (Germany) under contract 2008FE0070, and National Natural Science Foundation of China under Grant No. 11104298 and U1332202, the Innovation Program of Shanghai Institute of Ceramics under grant no.Y34ZC130G.

Notes and references

[a] *School of Materials Science and Engineering, Shanghai University, Shanghai, 200072, P. R. China. E-mail: zhangzhijun@shu.edu.cn, jtzhao@shu.edu.cn*
[b] *Energy Materials and Devices, Department of Chemical Engineering and Chemistry, Eindhoven University of Technology, P.O. Box 513, 5600 MB Eindhoven, the Netherlands.*
[c] *Luminescent Materials Research Group, Delft University of Technology, Mekelweg 15, 2629 JB Delft, the Netherlands. E-mail: P.Dorenbos@tudelft.nl*

1. M. Zeuner, S. Pagano and W. Schnick, *Angew. Chem. Int. Ed.*, 2011, **50**, 7754-7775.
2. C. Hecht, F. Stadler, P. J. Schmidt, J. S. auf der Günne, V. Baumann and W. Schnick, *Chem. Mater.*, 2009, **21**, 1595-1601.
3. J. Ruan, R. J. Xie, N. Hirosaki and T. Takeda, *J. Am. Ceram. Soc.*, 2011, **94**, 536-542.
4. J. Ruan, R. J. Xie, S. Funahashi, Y. Tanaka, T. Takeda, T. Suehiro, N. Hirosaki and Y. Q. Li, *J. Solid. State. Chem.*, 2013, **208**, 50-57.
5. Z. J. Zhang, O. M. ten Kate, A. C. A. Delsing, Z. Y. Man, R. J. Xie, Y. F. Shen, M. J. H. Stevens, P. H. L. Notten, P. Dorenbos, J. T. Zhao and H. T. Hintzen, *J. Mater. Chem. C.*, 2013, **1**, 7856-7865.
6. Y. Q. Li, G. de With and H. T. Hintzen, *J. Lumin.*, 2006, **116**, 107-116.
7. Y. Q. Li, J. E. J. van Steen, J. W. H. van Krevel, G. Botty, A. C. A. Delsing, F. J. DiSalvo, G. de With and H. T. Hintzen, *J. Alloy. Compd.*, 2006, **417**, 273-279.
8. K. Uheda, N. Hirosaki, Y. Yamamoto, A. Naito, T. Nakajima and H. Yamamoto, *Electrochem. Solid. St.*, 2006, **9**, H22-H25.
9. Y. Q. Li, N. Hirosaki, R. J. Xie, T. Takeda and M. Mitomo, *Chem. Mater.*, 2008, **20**, 6704-6714.
10. C. J. Duan, X. J. Wang, W. M. Otten, A. C. A. Delsing, J. T. Zhao and H. T. Hintzen, *Chem. Mater.*, 2008, **20**, 1597-1605.
11. R. J. Xie, N. Hirosaki, M. Mitomo, K. Sakuma and N. Kimura, *Appl. Phys. Lett.*, 2006, **89**, 241103.
12. H. L. Li, G. H. Zhou, R. J. Xie, N. Hirosaki, X. J. Wang and Z. Sun, *J. Solid. State. Chem.*, 2011, **184**, 1036-1042.
13. Y. Q. Li, G. de With and H. T. Hintzen, *J. Mater. Chem.*, 2005, **15**, 4492-4496.
14. Y. Q. Li, A. C. A. Delsing, G. de With and H. T. Hintzen, *Chem. Mater.*, 2005, **17**, 3242-3248.
15. N. Hirosaki, R. J. Xie, K. Kimoto, T. Sekiguchi, Y. Yamamoto, T. Suehiro and M. Mitomo, *Appl. Phys. Lett.*, 2005, **86**, 211905.
16. R. J. Xie, N. Hirosaki, M. Mitomo, K. Uheda, T. Suehiro, X. Xu, Y. Yamamoto and T. Sekiguchi, *J. Phys. Chem. B.*, 2005, **109**, 9490-9494.
17. Y. Q. Li, G. de With and H. T. Hintzen, *J. Electrochem. Soc.*, 2006, **153**, G278-G282.
18. R. D. Shannon, *Acta Crystallogr A.*, 1976, **32**, 751-767.
19. N. Yamashita, *J. Phys. Soc. Jpn.*, 1973, **35**, 1089-1097.
20. J. L. Sommerdijk, A. Bril and A. W. de Jager, *J. Lumin.*, 1974, **8**, 341-343.
21. P. Dorenbos, *J. Lumin.*, 2000, **91**, 155-176.

Cite this: DOI: 10.1039/c0xx00000x

www.rsc.org/xxxxxx

ARTICLE TYPE

22. P. Dorenbos, *J. Lumin.*, 2000, **91**, 91-106.
23. P. Dorenbos, *J. Lumin.*, 2000, **87-9**, 970-972.
24. Q. H. Zeng, Z. W. Pei, S. B. Wang, Q. Su and S. Z. Lu, *J. Phys. Chem. Solids.*, 1999, **60**, 515-520.
25. H. B. Liang, Q. H. Zeng, T. D. Hu, S. B. Wang and Q. Su, *Solid. State. Sci.*, 2003, **5**, 465-467.
26. Z. J. Zhang, O. M. ten Kate, A.C.A. Delsing, E. van der Kolk, P. H. L. Notten, P. Dorenbos, J. T. Zhao and H. T. Hintzen, *J. Mater. Chem.*, 2012, **22**, 9813-9820.
27. A. M. Srivastava and P. Dorenbos, *J. Lumin.*, 2009, **129**, 634-638.
28. P. Dorenbos, *J. Phys.:Condens. Matter.*, 2003, **15**, 8417-8434.
29. P. A. M. Berdowski, M. J. J. Lammers and G. Blasse, *J. Chem. Phys.*, 1985, **83**, 476-479.
30. L. G. Van Uitert and L. F. Johnson, *J. Chem. Phys.*, 1966, **44**, 3514-3522.
31. P. Dorenbos, *J. Phys.:Condens. Matter.*, 2003, **15**, 575-594.
32. P. Dorenbos, *J. Alloy. Compd.*, 2009, **488**, 568-573.
33. O. M. ten Kate, Z. Zhang, P. Dorenbos, H. T. Hintzen and E. van der Kolk, *J. Solid. State. Chem.*, 2013, **197**, 209-217.

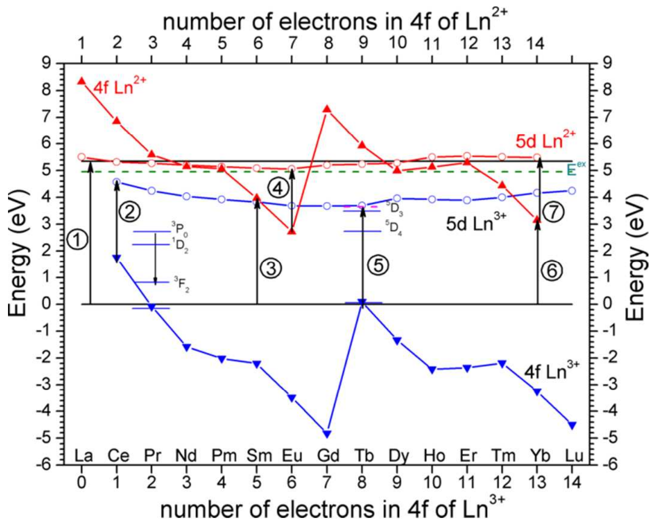
number of electrons in 4f of Ln2+
4f Ln2+
5d Ln2+
5d Ln3+
4f Ln3+
Energy (eV)
La Ce Pr Nd Pm Sm Eu Gd Tb Dy Ho Er Tm Yb Lu
number of electrons in 4f of Ln3+